Image processing of fabric evolution in granular salt subject to diffusive mass transfer

C. Zhu & C. Arson
School of Civil and Environmental Engineering, Georgia Institute of Technology, Atlanta, GA, USA
S.H. Jeong
School of Electrical and Computer Engineering, Georgia Institute of Technology, Atlanta, GA, USA
M. Dutta
School of Computer Sciences, Georgia Institute of Technology, Atlanta, GA, USA

ABSTRACT: Because of its favorable creep properties and low gas permeability, salt rock is viewed as an attractive host medium for nuclear waste disposals and natural resources storage. Under high stress and temperature conditions, diffusive mass transfer in salt rock can result in crack rebonding and strength recovery. In order to track the evolution of voids between salt crystals with lower load levels but higher healing rates than what is practically encountered in underground storage, we carried out creep loading tests on table salt. We used different loading conditions and inclusion materials to study the potential recurrence of topological patterns at grain boundaries. We developed a dedicated multi-stage image processing procedure to enhance microscopic image quality, and presented a slicing method to track the evolution of microstructure in different sections of the sample. This allowed us to analyze not only the evolution of average void size and orientation, but also the evolution of the fabric. We found that creep deformation is due to pore shrinkage along a diagonal direction across the sample, without significant grain rearrangement. It was noted however that basalt and sand inclusions rotated during the first 136 days of the creep tests. The proposed image processing techniques presented herein are expected to provide a methodology to track the evolution of microstructure descriptors that can be used to define alternative fabric tensors in thermodynamic models.

1 INTRODUCTION

Salt rock is viewed as a potential host medium for nuclear waste disposals, oil and gas storage, and more recently, compressed air energy storage. Salt rock caverns could ensure fluid containment because of the favorable creep properties and low permeability of halite (Cosenza et al. 1999, Berest et al. 2007, Chan et al. 2001, Kim et al. 2012). Main mechanisms of creep processes in halite are glide, cross-slip, diffusion, and dynamic recrystallization. Researchers, including Senseny et al. (1992) and Fam et al. (1998), characterized these mechanisms experimentally in halite, which occur over different ranges of temperature and pressure. At low pressure, dislocations and strain incompatibilities among grains induce stress concentrations, resulting in dilatant micro-cracking. In contrast, diffusive mass transfer (DMT) induces creep strain and also accelerates crack healing through local transfer of mass. For salt rock at room temperature, under high stress, crack rebonding and mechanical recovery induced by DMT occur within a few days. At higher temperature, the DMT process can easily accelerate, which is beneficial for the sustainability of geological storage facilities in salt rock.

Voyiadjis et al. (2011) categorized self-healing systems into two groups: damage-mechanisms-triggered active systems and external-simulation-induced passive systems. The authors previously proposed a thermo-mechanical model coupling crack debonding, opening, closure, and rebonding (Zhu & Arson 2014), which belongs to a uncoupled passive system, analogous to the close-then-heal mechanism proposed by Li & Uppu (2010). Microstructure descriptors used in the damage and healing model included void area and void projected length. Experimental results did not allow the continuous observation of a given section of the sample, which made it impossible to track fabric changes such as packing or grain re-arrangement.

In this paper, we propose advanced microscope post-processing techniques to track the evolution of grain boundaries during creep tests. Table salt grain boundaries are viewed as an analog of micro-cracks in salt rock. Image analysis will further support the development of thermodynamic models of fabric evolution during damage and healing around underground cavities. Section 2 describes the details of the experimental set up. Section 3 explains the procedure of grain boundary detection. Section 4 presents the technique of image processing for microstructure characterization. Section 5 summarizes the phenomenon observed through microscopic observa-

tions and the fabric changes obtained from image processing.

2 EXPERIMENTAL SET UP

We carried out creep tests on table salt under temperature and humidity controlled conditions (22^0C, 30%). The basic set up was described in (Zhu & Arson 2014) and is illustrated in Figure 1: table salt was encapsulated in acrylic tubes with nailed platens at the top and bottom. A spring located between the sample and the top platen was used to apply an axial compression. We assumed (and verified experimentally) that the length of the spring remained almost constant during the experiments, which put us in the conditions of constant stress creep conditions. The initial length of the samples was 20 mm.

In our previous study (Zhu & Arson, 2014), we were faced with some difficulties in characterizing table salt microstructure evolution, due to the lack of contrast between grains and boundaries. Moreover, it was difficult to track the movement and shape changes of specific grains from sequential microscope observations, because all grains were similar in size, shape and orientation; as a result, the methodology proposed was appropriate to characterize average grain and pore shapes and sizes, but not to track the evolution of grain-to-grain or pore-to-pore distances.

In the set up used herein, we mixed table salt with inclusions that were used as reference points of observation. We used basalt (green) and colored sand (red) because they can be easily purchased with specific sizes or shapes, do not interact with table salt, and are easy to be dyed into other colors. The mass of the inclusions amounted to 5% of the total mass of the samples. Table 1 summarizes inclusions basic properties. We estimated roundness and sphericity parameters according to the criteria by Krumbein & Sloss (1963): sand particles are larger and more rounded than basalt particles. The presence of colored inclusions enabled us to study grain rearrangement and boundary rebonding around controlled microstructure irregularities. More importantly, because salt grains are transparent and difficult to distinguish, inclusion particles help tracking the microstructure evolution of a certain area during continuous observation. We subjected our salt, salt and basalt and salt and sand samples to three different creep loadings (0.3, 0.4, and 0.5 MPa), as shown in Figure 1.

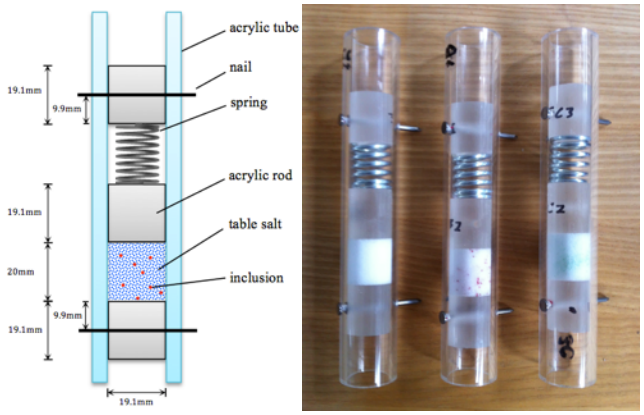

Figure 1. Set up of creep tests: pure salt, salt with sand, and salt with basalt (from left to right).

Table 1. Basic properties of inclusion particles used in this study

Particle type	Color	Roundness	Sphericity	Feret's diameter (mm)	Aspect ratio R
Sand	red	0.3~0.7 (subangular to rounded)	0.5~0.9	0.6~1	0.6~1
Basalt	green	0.1~0.7 (very angular to rounded)	0.3~0.8	0.1~0.5	0.2~1

Samples were put in a sealed container, under temperature and humidity controlled conditions. During the first three months of the creep experiment, we maintained dry conditions. Although later we started to maintain a humid environment, as explained in Wexler & Hasegawa (1954), this paper mainly focuses on the microscopic observations obtained during the dry condition period.

3 GRAIN BOUNDARY DETECTION

We measured the length of the samples and observed the table salt granular assembly under the microscope at regular time intervals. Time intervals were shorter at the beginning of the experiment, in order to better capture the fast microstructure changes at the beginning of creep deformation.

Table salt particles are transparent cubic grains with planar surfaces. Light can easily penetrate through or get reflected, which largely impairs the quality of microscopic images. We present an edge detection technique that allowed us to enhance the contrast between grains and voids. The image-processing algorithm was implemented in *MATLAB*.

We first passed the microscopic images through an initial filter called *ContrastUp,* which enhances the contrast. *ContrastUp* calculates the average distance between pixel values, and assigns a new set of pixel values to the image in order to increase the average distance between pixels. We used a Gaussian distribution measure to determine the maximum, minimum, mean, and standard deviation of the pixel values in the image. Built-in functions implemented in *MATLAB* allowed us to control the intensity of the contrast filter.

After filtering the original image with *ContrastUp* in order to enhance the contrast, we dismantled the image into three layers (or matrices) of red, green, and blue (RGB) pixel values (Figure 2). The main purpose of the separation into RGB layers is to determine the pixel color for which the matrix contrast is the highest. For each layer, the image can be turned into gray-scale because it is composed of only one color matrix. We created three new gray-scale images after separation, which resulted in the processing of four images after RGB layer separation.

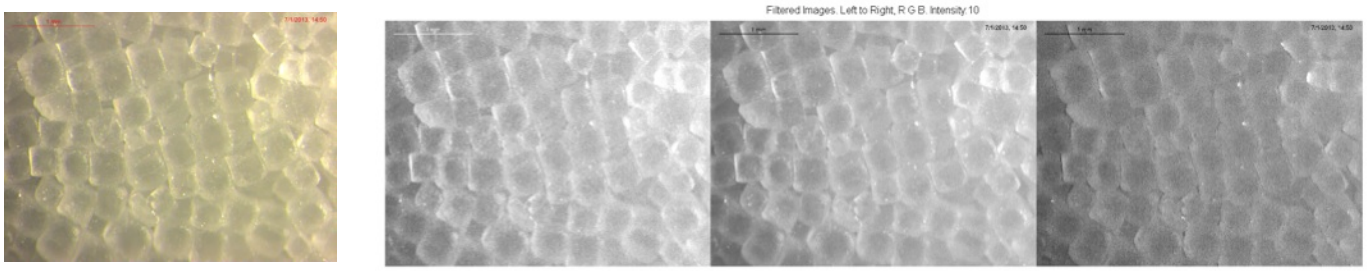

Figure 2. Salt Sample image passed through *ContrastUp* and *RGB MATLAB* filters

We developed an edge detection program, based on *MATLAB Edgetrace* function, which successfully detects variations in pixel values. The filter goes through each pixel of the image, and highlights diagonally adjacent pixels if they differ greatly in pixel values. The problem with this method is that since pixel values vary significantly when measured individually, areas with tiny variations in pixel values are also highlighted. In order to address this problem, we modified *Edgetrace* in order to make the filter go through groups of four adjacent regions (forming a square, as shown in figure 3), instead of four adjacent pixels. The program calculates the mean pixel value of the area covered by the four regions and by the eight surrounding subsections (as shown in figure 3). The square formed by the four regions is detected as an edge region if the mean pixel value of the regions differs greatly from the mean pixel value of the large area covered by the regions and the subsections. If the square formed by the four regions is detected as an edge region, then the program detects a region as an edge if the difference between the mean pixel value of that region and the mean pixel value of the area covered by the regions and the subsections exceeds a certain threshold. For instance, by checking with the threshold, three regions (three small squares) can be detected as an edge. Highlighting three regions presents a trend, which agrees well with the real grain boundary indicated by the red curve (Figure 3). By this means, we always look at a larger region for boundary detection.

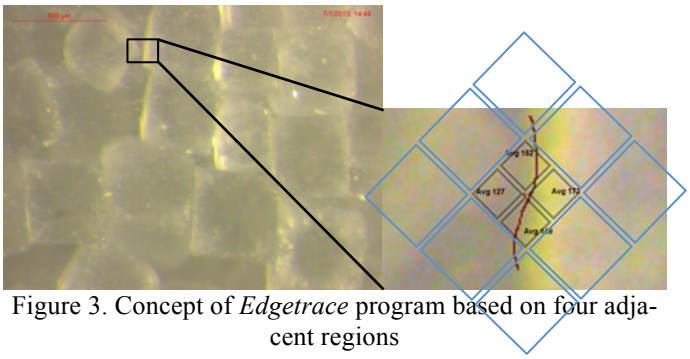

Figure 3. Concept of *Edgetrace* program based on four adjacent regions

Because of the poor image quality, color differences between regions are usually insignificant. In order to overcome this problem, we developed a multi-threshold overlapping program, which compares the difference between pixel color values to a threshold value. If the threshold value is exceeded, the program recognizes the pixel as part of a boundary. Multi-threshold overlapping creates multiple images from the original using different threshold values (Figure 4). Overlapping multiple images creates the final image containing a more accurate description of grain boundaries. The binary image obtained after the multi-threshold process provides us an image with clearer boundaries. Note that for areas with strong light intensities, the results are not satisfactory. We are currently working on that issue and also improving the technique to connect the neighboring pixels and present the boundary outlines directly.

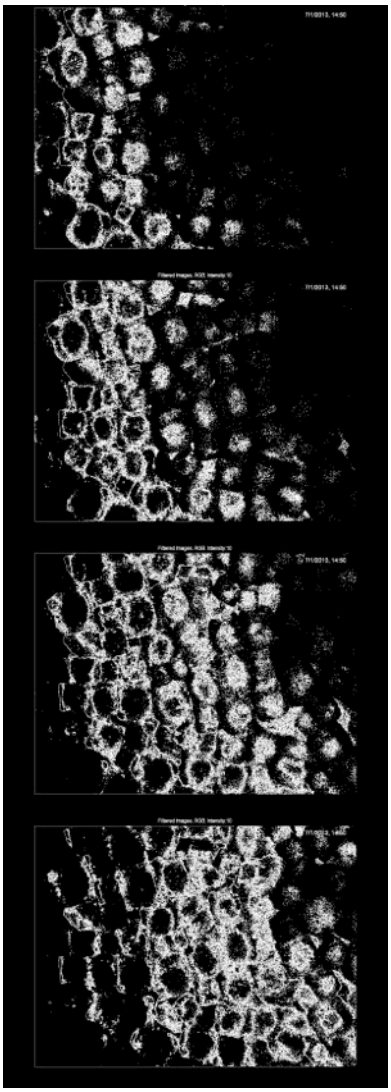

Figure 4. Salt sample image processed by the multi-threshold program (from top to bottom: original, red, green, and blue layers, respectively)

4 FABRIC CHARACTERIZATION

As a complement of the grain boundary detection program developed in *MATLAB*, we also processed the microscopic images with *ImageJ* application, which is a Java-based image-processing program developed by Abramoff et al. (2004). In addition to the powerful image processing tools, *ImageJ* allows developing plugins to meet our own requirements.

In our previous study (Zhu & Arson 2014), we used *ImageJ* to capture characteristics of voids between salt grains, and we used the probability density functions of the void area and projected length to define damage and healing. Because we did not have a set of images on a given area of the sample, it was impossible to get relevant statistical data on packing, grain arrangement or similar fabric information. In the present study, we used inclusions as reference points in our image analysis. This reference inclusion particle is equivalent to the origin of a Eulerian coordinate system. In order to compare the evolution of microstructure within a given sample area, we wrote plug-ins that fixed the dimensions of the image used for analysis. A scale plug-in allowed us to obtain the actual size of the microscope images (Figure 5). A second plug-in allowed us to choose the size of the image so as to ensure the representativeness of the grain distribution: Figure 6 shows an example, in which the initial image was cropped to achieve a size of 5mm by 4mm.

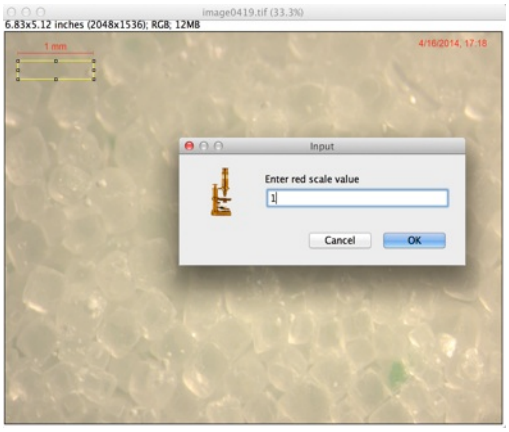

Figure 5. Scale plug-in: measure of the dimensions of the microscope images.

Subsequent image processing involved removing backgrounds, adjusting color threshold, making binary images, and inverting colors. We obtained a preliminary binary image of poor quality, because of light reflection and transmission in the bulk of salt grains. In order to overcome this problem, we designed an additional procedure for image analysis, in order to remove outliers: the quality of the image was improved. Inclusions used in the experiments were either red or green, and could be recognized as voids by the program. To avoid this situation, we wrote another plug-in in *ImageJ*, which assigned the mean pixel value of a salt grain to the region occupied by the inclusion (which we highlighted manually). By so doing, inclusion particles were treated as solid components (Figure 7). Figure 8 illustrates the image processing steps to get a binary image with *ImageJ*.

Figure 6. Cropped image with size 5mm by 4mm, centered at a green basalt particle

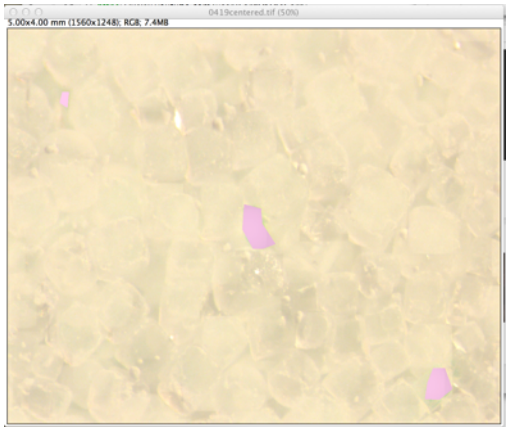

Figure 7. *ImageJ* plug-in written to identify inclusions as solid grains.

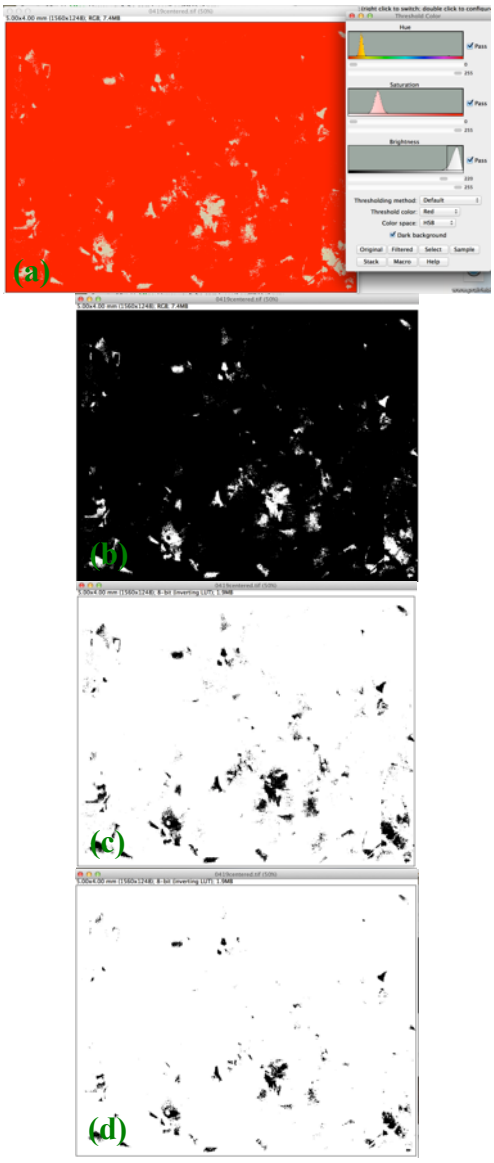

Figure 8. Main image post-processing steps to get a binary image with *ImageJ*: (a) adjust color threshold, (b) binary image, (c) invert black and white regions, (d) filter and remove outliers.

In order to study not only the evolution of average void distributions, but also the evolution of the fabric (e.g., packing, grain arrangement), we developed a slicing method, by which a microscopic image is evenly cut into a few sections (Figure 9). The choice of the number of sections is critical. With too few sections, the slicing refinement will not be high enough to capture the relative fabric changes throughout the sample. With too many sections, the number of voids in each section will not be sufficient for statistical analysis. In each section, we define a representative void postulated of a circular shape, the area of which is equal to the total area of voids in the slice, and the centroid of which is calculated as the average position of all voids centroids in the sample. The coordinates of the representative void are:

$$X = \frac{\sum_{i=1}^{n} A_i x_i}{\sum_{i=1}^{n} A_i}, \quad Y = \frac{\sum_{i=1}^{n} A_i y_i}{\sum_{i=1}^{n} A_i}, \tag{1}$$

in which A_i stands for the area of the ith void, x_i and y_i are the coordinates of the ith void in the current section. Sample compactness is estimated from the distance between representative voids.

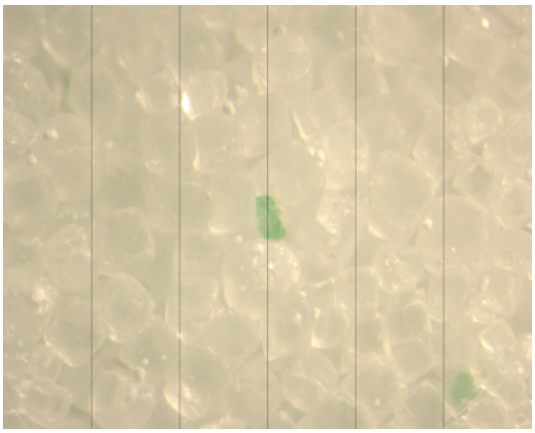

Figure 9. Division of six sections for analyzing fabric evolution

The flow chart in figure 10 summarizes the main steps of image processing using *ImageJ*.

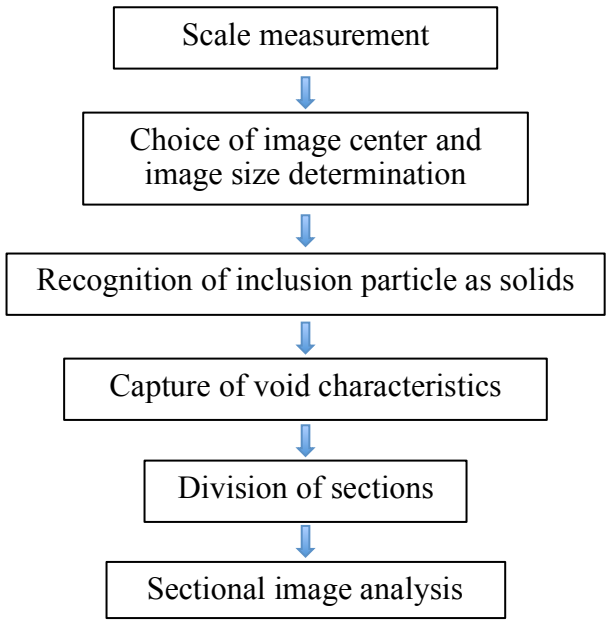

Figure 10. Image processing steps.

5 PRELIMINARY RESULTS AND DISCUSSION

Creep processes depend on stress, humidity, and temperature conditions. In dry conditions, grain boundary rebonding is slow, which explains the absence of significant fabric changes observed during the first 136 days of the experiment (Figure 11). Some inclusion particles rotate or move, due to grain re-arrangement. Such grain movement can only be captured and characterized through image analysis (Figure 12).

Compared to basalt inclusions, sand inclusions do not change significantly in orientation or position. Sand particles are larger than basalt grains. As a result, the coordination number of a sand particle (7~10) is higher than that of a basalt particle (3~6), which implies that grain boundary friction is higher with sand, which largely impedes the movements of sand inclusions.

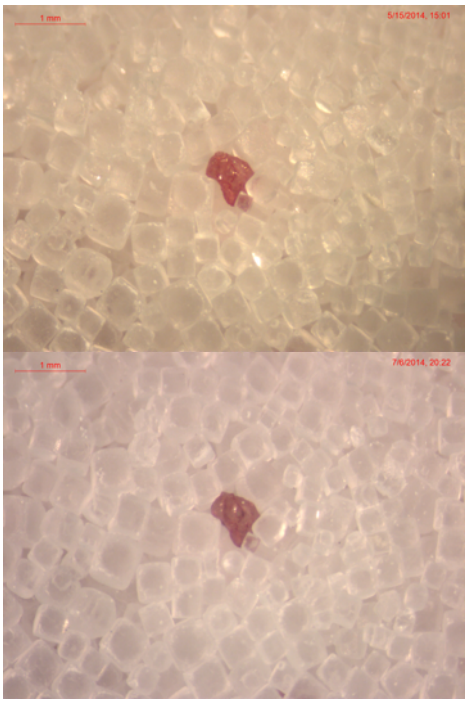

Figure 11. Continuous microscopic observation of salt microstructure during creep tests, with sand inclusions: no obvious fabric change. Top: after 40 days. Bottom: after 92 days.

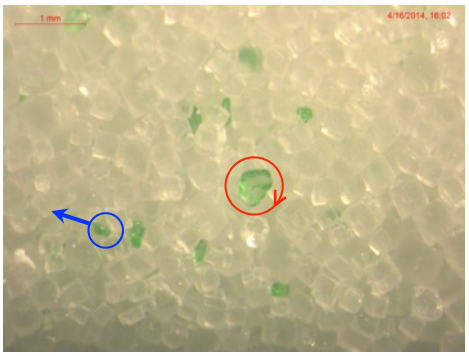

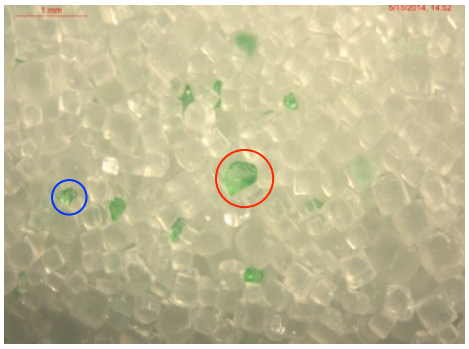

Figure 12. Rotation and movement of inclusion particles observed within the same region. Top: after 11 days. Bottom: after 40 days.

We carried out continuous length measurements on nine samples, described in Table 2. Measurement results verify that the creep process is extremely slow under the current loading and humidity conditions. Sample shortening is within a millimetric scale. Samples without any inclusions (i.e., pure table salt grains) creep faster than those mixed with sand or basalt particles, and are less sensitive to loading conditions. The relatively angular shape of the inclusion particles contributes to these phenomena: inclusions actually prevent table salt grains from sliding along their planar surfaces.

Table 2. Sample length change due to creep after 136 days under constant loading

Creep Load / Specimens	0.3MPa	0.4MPa	0.5MPa
Pure table salt	0.4 mm	0.3 mm	0.8 mm
Table salt + sand	0.2 mm	0.1 mm	0.1 mm
Table salt + basalt	0.1 mm	0.1 mm	0.1 mm

We present below the results obtained with our slicing technique for mixtures containing basalt grains: Table 3 summarizes the characteristics of voids within each individual section, and also the evolution of the centroid-to-centroid distance of the representative voids in the slices. We compared two images (5mm by 4mm) acquired after 11 days and 92 days, and performed an analysis with six slices (Figure 13).

Table 3. Summary of void characteristics obtained with the slicing method

Section No.	Number of voids	Centroid x-coordinate (mm)	Centroid y-coordinate (mm)	Total area (mm^2)	Average area (mm^2)	Porosity
Microscopic image taken at 11 days (276 voids)						
1	47	0.38	2.709	0.09	0.002	0.027
2	29	1.413	3.041	0.111	0.004	0.033
3	48	2.194	2.286	0.075	0.002	0.023
4	69	3.035	2.888	0.18	0.003	0.054
5	36	4.074	2.928	0.047	0.001	0.014
6	47	4.688	3.04	0.129	0.003	0.039
Microscopic image taken at 92 days (280 voids)						
1	40	0.26	2.994	0.058	0.001	0.017
2	69	1.42	2.913	0.081	0.001	0.024
3	30	2.341	2.115	0.065	0.002	0.02
4	57	3.178	2.777	0.05	8.85E-04	0.015
5	56	4.132	2.242	0.05	8.86E-04	0.015
6	28	4.775	3.072	0.062	0.002	0.019

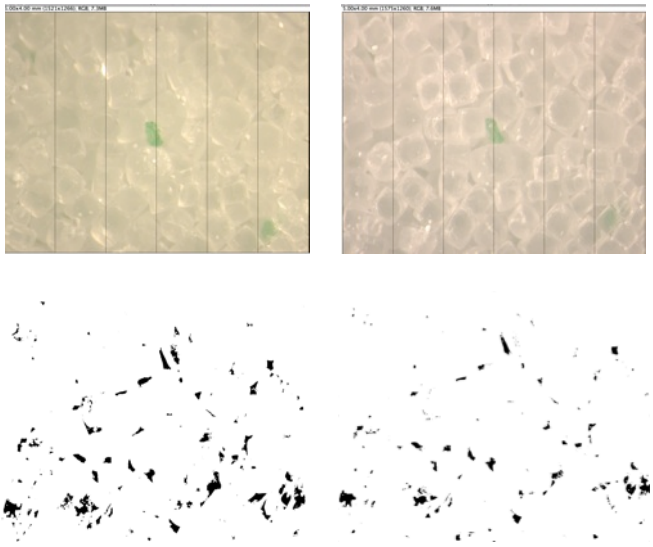

Figure 13. Comparison of void characteristics obtained from microscopic observation after 11 days (left) and 92 days (right): microscope images (top) and binary images (bottom).

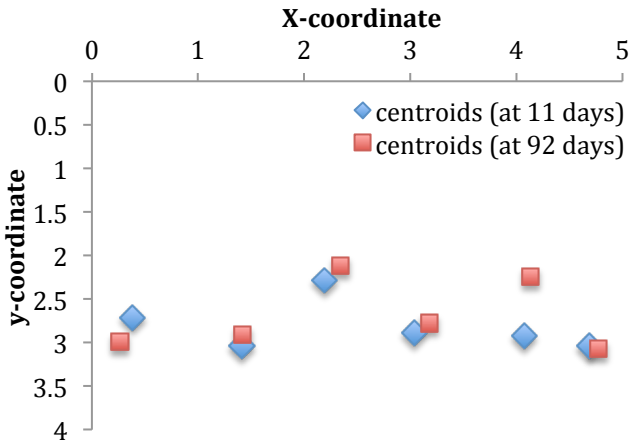

Figure 14. Evolution of the positions of representative void centroids during the tests.

Results indicate that the relative distance between centroids did not change considerably, and that the average area of the voids significantly decreased in all slices. This indicates that samples shorten without significant grain rearrangement, which substantiates the qualitative observation made earlier, where no major fabric changes were noted. Another trend is that voids shift not only along the horizontal axis (i.e., the creep loading direction) but also along the vertical axis (Figure 14), which implies that the force field in our observational area points aligns along a diagonal direction. Future observation will also concentrate on a larger region to check if the main direction of the force field is along the horizontal direction. Our future research investigations will aim to relate the fabric parameters and the field of micro-forces to a thermodynamic model of damage and healing.

6 CONCLUSIONS

We conducted creep tests on granular assemblies made of table salt, table salt mixed with basalt grains, and table salt mixed with colored sand grains. Basalt and sand inclusions represented 5% of the mass of the samples, and were used as reference points in our image analysis. We developed two post-processing tools. The edge detection tool (programmed in *MATLAB*) enhances contours and improves the detection of grain boundaries. Plug-ins written in *ImageJ* calculate equivalent void properties in different sections of the image, which serves as a basis to analyze fabric evolution over time.

Under ambient humidity and temperature conditions, and for the stresses imposed during the tests, creep rates were slow, so that no obvious salt fabric changes were noted. Moreover, we observed and measured that the presence of inclusions slowed down the rate of deformation, and reduced the sensitivity of the results to the loading stress. We attributed these phenomena to the increased friction be-

tween particles making the assembly when angular inclusions with higher coordination number that salt grains are present in the sample. Using inclusion particles proved to be an efficient technique to track the evolution of salt fabric. Our future studies will include tests performed in various humidity and temperature conditions, in order to explore fabric changes under higher creep deformation rates. In ambient temperature and humidity conditions, we found that creep deformation is due to pore shrinkage along a diagonal direction across the sample, without significant grain rearrangement. It was noted however that basalt and sand inclusions rotated during the first 136 days of the creep tests.

We are currently working on a machine-learning algorithm, in order to allow *ImageJ* to automatically distinguish grains and voids, with no further filtering during image post-processing. Table salt boundaries are viewed as an analog of micro-cracks in salt rock. Image analysis will further support the development of thermodynamic models of fabric evolution during damage and healing around underground cavities. We will focus our next modeling effort on grain-boundary diffusion, and study the micro-level processes including solid-fluid chemical interactions. The proposed image processing techniques presented herein are expected to provide a methodology to track the evolution of microstructure descriptors that can be used to define alternative fabric tensors in thermodynamic models.

ACKNOWLEDGEMENT

The authors are grateful to Professor Santamarina at the Georgia Institute of Technology, who kindly gave access to his laboratory for microscope imaging, and made suggestions to improve the experimental set up. The authors also would like to acknowledge the financial support for this research from the School of Civil and Environmental Engineering at the Georgia Institute of Technology, and the National Science Foundation (Grant No. CMMI-1362004/1361996).

REFERENCES

Abramoff, M.D., Magalhaes, P.J. & Ram, S.J. 2004. Image processing with *ImageJ*. *Biophotonics international.* 11(7): 36–42.

Berest P., Brouard B., Karimi-Jafari M., & Van Sambeek L. 2007. Transient behavior of salt caverns—interpretation of mechanical integrity tests. *International Journal of Rock Mechanics and Mining Science*. 44(5): 767–786.

Chan K., Bodner S., & Munson D. 2001. Permeability of WIPP salt during damage evolution and healing. *International Journal of Damage Mechanics.* 10(4): 347–375.

Cosenza P., Ghoreychi M., Bazargan-Sabet B., & De Marsily G. 1999. In situ rock salt permeability measurement for long-term safety assessment of storage. *International Journal of Rock Mechanics and Mining Science*. 36(4): 509–526.

Fam, M., Santamarina, J., & Dusseault, M. 1998. Wave-based monitoring processes in granular salt. *Journal of Environmental & Engineering Geophysics*. 3(1): 41-47.

Kim H.M., Rutqvist J., Ryu D.W., Choi B.H., Sunwoo C., & Song W.K. 2012. Exploring the concept of compressed air energy storage (caes) in lined rock caverns at shallow depth: a modeling study of air tightness and energy balance. *Applied Energy*. 92: 653–667.

Krumbein, W.C. & Sloss, L.L. 1963. *Stratigraphy and Sedimentation* (2nd edition). Freeman, San Francisco.

Li, G. & Uppu, N. 2010. Shape memory polymer based self-healing syntactic foam: 3-D confined thermo-mechanical characterization. *Composites Science and Technology*. 70(9): 1419–1427.

Senseny, P., Hansen, F., Russell, J., Carter, N., & Handin, J. 1992. Mechanical Behavior of rock salt: phenomenology and micromechanisms. *International Journal of Rock Mechanics and Mining Sciences & Geomechanics Abstracts*. 29(4): 607-619.

Wexler, A. & Hasegawa, S. 1954. Relative humidity temperature relationships of some saturated salt solutions in the temperature range 0^0C to 50^0C. *Journal of Research of the National Bureau of Standards*. 53(1): 19-26.

Voyiadjis G.Z., Shojaei A., & Li G. 2011. A thermodynamic consistent damage and healing model for self healing materials. *International Journal of Plasticity*. 27(7):1025–1044.

Zhu, C. & Arson, C. 2014. A model of damage and healing coupling halite thermo-mechanical behavior to microstructure evolution. *Geotechnical and Geological Engineering, Special Issue: Thermo-hydro-mechanical behavior of soils and energy geostructures*. DOI: 10.1007/s10706-014-9797-9.